Acta Crystallographica Section D
Biological Crystallography
ISSN 0907-4449

Development of high-performance X-ray transparent crystallization plates for *in situ* protein crystal screening and analysis

Ahmed S. M. Soliman,[a] Matthew Warkentin,[a] Benjamin Apker[b] and Robert E. Thorne[a,b]*

[a]Department of Physics, Cornell University, Ithaca, New York, USA, and [b]MiTeGen LLC, Ithaca, New York, USA

Correspondence e-mail: ret6@cornell.edu

Received 28 January 2011
Accepted 17 May 2011

X-ray transparent crystallization plates based upon a novel drop-pinning technology provide a flexible, simple and inexpensive approach to protein crystallization and screening. The plates consist of open cells sealed top and bottom by thin optically, UV and X-ray transparent films. The plates do not need wells or depressions to contain liquids. Instead, protein drops and reservoir solution are held in place by rings with micrometre dimensions that are patterned onto the bottom film. These rings strongly pin the liquid contact lines, thereby improving drop shape and position uniformity, and thus crystallization reproducibility, and simplifying automated image analysis of drop contents. The same rings effectively pin solutions containing salts, proteins, cryoprotectants, oils, alcohols and detergents. Strong pinning by rings allows the plates to be rotated without liquid mixing to 90° for X-ray data collection or to be inverted for hanging-drop crystallization. The plates have the standard SBS format and are compatible with standard liquid-handling robots.

1. Introduction

The growth and harvesting of protein crystals remains a major bottleneck in the pipeline from gene to three-dimensional molecular structure and from structure to pharmaceutical therapy (McPherson, 1999; Bergfors, 1999; Berry *et al.*, 2006; Chayen, 2007, 2009; Li & Ismagilov, 2010). Protein crystallization is commonly performed using the sitting-drop vapor-diffusion method (McPherson, 1999; Chayen & Saridakis, 2008). Microlitre to nanolitre drops of protein-containing solution and much larger volumes of precipitant-containing reservoir solution are dispensed into an injection-molded multiple-well plastic plate and the plate is then sealed using plastic film. As the protein drop equilibrates with the reservoir solution, the protein concentration increases until, in favorable cases, crystal nucleation and growth occur. A large number of plate designs are available, varying principally in well size, shape and number (Korczyńska *et al.*, 2007).

Pre-formulated crystallization screens (Jancarik & Kim, 1991) that sparsely sample mixtures of a wide range of crystallization solution components have simplified the search for crystallization conditions. Systems for automated liquid and plate handling, for automated imaging and image analysis (Stevens, 2000; Cumbaa *et al.*, 2003; Walter *et al.*, 2005; Berry *et al.*, 2006; Hiraki *et al.*, 2006) and for *in situ* X-ray diffraction screening of crystallization outcomes (Watanabe *et al.*, 2002; Jacquamet *et al.*, 2004; Yadav *et al.*, 2005; Eisenstein, 2007; Skarzynski, 2009) have reduced the amount of human effort required. However, the search for diffraction-quality crystals is still time-consuming and expensive.

© 2011 International Union of Crystallography
Printed in Singapore – all rights reserved

Alternative approaches based upon microfluidic 'chips' or 'cards' (Hansen *et al.*, 2002, 2006; Zheng *et al.*, 2003; Sauter *et al.*, 2007; Shim *et al.*, 2007; Gerdts *et al.*, 2008; Leng & Salmon, 2009; Dhouib *et al.*, 2009; Li & Ismagilov, 2010) can implement microbatch, liquid–liquid diffusion, free-interface diffusion and dialysis crystallization. Protein and precipitant solutions are combined and/or distributed to different parts of the chip using microfluidic mixers and valves. Volumes per crystallization condition can be very small (1–10 nl), allowing a very large number of closely spaced conditions to be explored using little protein and rapid identification of optimum crystallization conditions once an initial hit has been obtained. Modest polymer thicknesses within the chips facilitate *in situ* X-ray examination. However, most current implementations are not suitable for initial screening using a random matrix of crystallization solutions. Because of the small crystallization solution volumes used, the crystals obtained are often too small for examination using laboratory X-ray sources. Because of water absorption by chip components, adsorption of protein on surfaces and differences in kinetics, conditions identified on chips often do not translate well to conventional larger-volume crystallization methods. Microfluidic approaches also require the use of specialized liquid-handling and chip/card manipulation, storage and imaging systems. Despite their considerable promise, microfluidic approaches have so far seen limited adoption.

Several groups have explored protein crystallization and *in situ* data collection using X-ray transparent glass or polymer capillaries (Gavira *et al.*, 2002; Yadav *et al.*, 2005; Kalinin *et al.*, 2005). This approach is cumbersome and should be more effectively implemented using microfluidic cards.

Rather than developing a technology that required a new supporting infrastructure, our goal was to use concepts from fluid and interface physics to produce an improved crystallization plate that is fully compatible with existing liquid and plate-handling hardware. Here, we describe the evolution and evaluation of our design, which uses strong contact line pinning instead of wells to define and confine the drops. The plate can be used for hanging and sitting drops of both soluble and membrane proteins and allows low-background *in situ* X-ray data collection with the plate held in any orientation.

1.1. Problems with current crystallization plates

The crystallization plates currently marketed for use with automated drop-dispensing systems are similar in their basic design and function (Korczyńska *et al.*, 2007). They have several shortcomings.

(i) Most plates implement the sitting-drop method. Sedimentation and adhesion of crystals to the plate surface makes them difficult to harvest, resulting in crystal damage and reduced yields. Inverting the plates to obtain hanging drops causes the contents of the reservoir and protein wells to spill out and mix [unless the reservoir is gelled (Whon *et al.*, 2009) or replaced by a dessicant (Lu *et al.*, 2010)].

(ii) The shapes and positions of the dispensed drops are irregular and irreproducible, complicating automated image analysis of drop contents. Protein drops tend to be drawn to the corners of flat-bottom wells, where they wet the side and bottom. Curved-bottom wells can improve drop shape and position reproducibility if the drops are carefully dispensed and the contact-angle hysteresis is small, but they complicate optical inspection. Drop positioning can be improved by matching the well size to the drop size, but this degrades the optics and makes harvesting difficult.

For soluble proteins, drop shape can be improved by using hydrophobic coatings, which reduce drop wetting to plate surfaces. However, drops slide more freely on hydrophobic surfaces and this degrades positional accuracy unless curved-bottom wells are used. Hydrophobic surfaces also make contact dispensing more difficult, because small drops may not form a strong enough contact to be released from the dispensing tip (Berry *et al.*, 2006).

(iii) Irregular shapes for both the protein drops and reservoir solution lead to irregular surface-to-volume ratios and thus irreproducible equilibration, nucleation and crystallization kinetics. Nucleation rates, which can vary from $\sim$1 nucleus per day to $\sim$1 nucleus per minute over a very small fractional change in supersaturation, are especially sensitive. Repeating and/or scaling up to larger volumes conditions that produce a 'hit' often yields no crystals or precipitate.

(iv) Because commercial plates are made of relatively thick and therefore strongly X-ray absorbing and scattering plastic, *in situ* X-ray diffraction cannot easily be used to assess crystallization outcomes (Eisenstein, 2007). Thick plastic also hinders the use of birefringence and UV spectroscopy to identify crystalline material in each drop (Bourgeois *et al.*, 2002). As a result, much time is wasted manually harvesting, soaking, mounting, flash-cooling and measuring the X-ray diffraction properties of crystals that are poorly ordered.

One commercial injection-molded plate, from NatX-ray and Greiner, has been specifically designed for X-ray inspection. The plate has 250 µm thick plastic windows sealing the bottom of the protein wells and a low profile that reduces obstructions to the diffracted X-rays. The scattering from the plastic is still excessive when searching for microcrystals produced in initial screening. The injection-molding methods required to further reduce the plastic thickness are presently unreliable and prohibitively expensive. Korczyńska *et al.* (2007) used thermoforming rather than injection molding to implement a plate with a 250 µm plastic thickness. With some modifications it could also be suitable for *in situ* X-ray inspection, but is somewhat cumbersome to use with standard plate-handling hardware.

These shortcomings of existing plates have a large negative impact on screening efficiency and on the overall throughput of structural genomics efforts.

1.2. Enhancing contact line pinning

The initial objective of our work was to identify a way to strongly pin the contact lines of dispensed drops at particular locations and thus obtain drops with well defined positions and shapes. The contact line defines the three-phase boundary

of liquid, solid substrate and air. In order for a drop to displace or spread on a solid surface, the contact line must depin and move.

On a flat surface, a drop's contact line will not advance (or recede) until the contact angle θ reaches the critical advancing angle θ_a (or receding angle θ_r). The condition for contact line stability is then $\theta_r < \theta < \theta_a$. The difference between the maximum advancing and minimum receding contact angles is the contact-angle hysteresis $\Delta\theta = \theta_a - \theta_r$ and is a measure of the strength of contact line pinning.

Drops dispensed on surfaces that provide large contact-angle hysteresis will be very stable against perturbations. However, because of shape dynamics during dispensing, the drops will often have irregular shapes: once the contact line becomes pinned it is unlikely to move even though this might result in a more symmetrical drop with a less distorted surface. Soluble protein drops dispensed onto hydrophobic surfaces (*e.g.* the coated surfaces of some commercial plates) tend to bead up rather than wet the surface and have somewhat more regular shapes. These surfaces give large advancing angles θ_a and receding angles θ_r but small contact-angle hysteresis $\Delta\theta = \theta_a - \theta_r$, so that the drops are unstable towards, for example, tilting.

Our first experiments attempted to confine drops by patterning hydrophilic disks on an otherwise hydrophobic surface (Berejnov & Thorne, 2005), a technique that has been widely used in biotechnology. Liquid dispensed onto the hydrophilic disk quickly spreads to its boundary. Further spreading requires addition of liquid until the contact angle exceeds the (large) maximum advancing value of the surrounding hydrophobic surface. When liquid is withdrawn from the drop, the contact line remains pinned at the boundary until the contact angle reaches the (small) minimum receding angle of the hydrophilic surface. Consequently, the contact-angle hysteresis is large, the drop's contact line is strongly pinned at the boundary and the maximum liquid volume that can be stably held to the area within the boundary is much larger than on an unpatterned surface. The drop's position and shape will then be determined by the circular boundary for a wide range of drop volumes.

However, surfaces with hydrophobic/hydrophilic patterning are easily contaminated and their properties tend to be unstable over time. The enhancement of contact line pinning also depends on the liquid composition: detergent-containing membrane-protein solutions will not be confined to hydrophilic disks but will quickly spread to the surrounding hydrophobic regions.

An alternative and much more robust approach for pinning liquid contact lines is based upon topographic rather than chemical patterning (Kalinin *et al.*, 2008, 2009). Liquid drops can be held in place using raised rings with steep side walls, which can be of the same material as the surrounding surfaces.

Fig. 1 shows a schematic diagram of a drop pinned to a ring with a trapezoidal cross-section. The key idea is that motion of the advancing contact line will occur only when the contact angle relative to the local surface, which may be inclined relative to the average surface, exceeds θ_a. Consequently, as liquid is added to the area defined by the ring it will spread to the inside wall and across the top of the ring before becoming pinned at the ring's outer wall, which is inclined relative to the average surface plane at angle φ. The maximum advancing angle relative to the average surface plane will be $\theta_a^* = \theta_a + \varphi$ and will thus be enhanced by the inclination angle φ. Similarly, the minimum receding contact angle relative to the average surface plane $\theta_r^* = \theta_r - \varphi$ will be reduced (with a minimum value of 0° when the ring height is much smaller than the drop height). The condition for stability of a drop confined by a ring is then $\theta_r^* = \theta_r - \varphi < \theta < \theta_a + \varphi = \theta_a^*$. The contact-angle hysteresis will thus be increased relative to a flat surface by as much as 2φ: a very large factor if the side walls are nearly vertical.

The bulging liquid dome that can be produced by carefully overfilling your coffee cup owes its stability to this physics. In this case, the 'ring' provided by the lip of the coffee cup is macroscopic. Kalinin *et al.* (2008, 2009) showed that the pinning strength, as measured by the maximum advancing contact angle, provided by a ring saturates at a ring height of only a few micrometres (at least for drops of volumes from $\sim$100 nl to $\sim$100 µl) and that the pinning strength is independent of ring width down to a similar length scale. As a result, rings with microscopic cross-sections can dramatically enhance the pinning and stability of millimetre-high drops on what are essentially flat surfaces. This allows the wells of conventional crystallization plates to be eliminated, with corresponding improvements in optics, and injection-molded bottoms of the plates to be replaced by highly X-ray transparent thin films.

2. Experiments and results: general

Our objective was to develop crystallization plates using Kalinin and coworkers' topographic drop-pinning (TDP) technology that were compatible with the standard SBS format and existing drop-dispensing and plate-handling hardware and that allowed *in situ* optical, UV and X-ray analyses of protein crystals. The plates implement the popular vapor-diffusion crystallization method, although they can also be used for microbatch crystallization. The wells used in conventional plates to contain the protein and reservoir solutions are replaced by micropatterned rings that strongly pin the liquid contact line to the ring. This strong pinning allows the plates to be inverted for hanging-drop crystallization and to be held in any orientation for X-ray data collection. It also produces drops with much more reproducible positions and shapes, simplifying automated image analysis of drop contents and improving the reproducibility of crystallization experiments. We next describe the evolution of our design.

3. Experiments and results: TDP crystallization plate prototype 1

Our first prototype was comprised of a 50 µm thick X-ray, UV and optically transparent PVC film attached to the

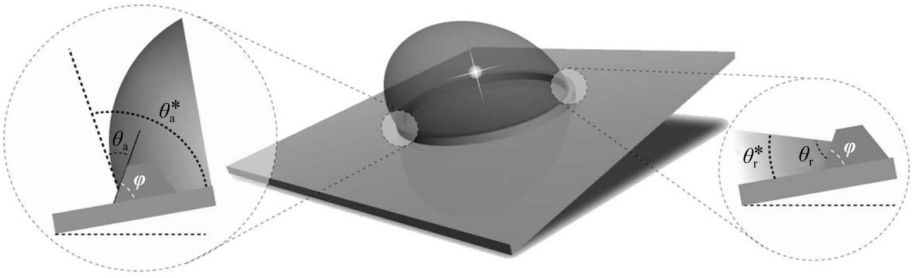

Figure 1
Schematic diagram of a drop on an inclined substrate pinned to a ring with side-wall angles φ. The maximum advancing angle θ_a^* (on the downhill side of the contact line) is increased from its value on a flat surface by φ. The minimum receding angle θ_r^* (on the uphill side) is reduced by φ (or to near 0°, whichever is larger) (Kalinin *et al.*, 2008).

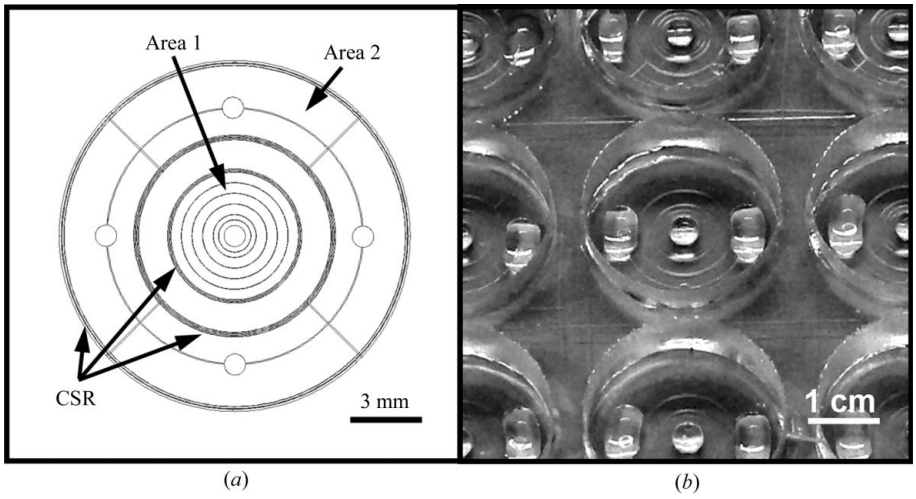

Figure 2
(*a*) Schematic diagram of the ring pattern in each cell of TDP crystallization plate prototype 1. Protein solution is dispensed in Area 1, which has a diameter of 6 mm and contains six 20 µm wide concentric rings to pin drops with a range of volumes. Reservoir solution is dispensed into each quadrant of the annular Area 2. Closely spaced rings (CSRs) bound each area and can catch and pin the contact line if it spreads owing to dust, ring defects or plate accelerations. (*b*) Plate prototype 1, consisting of a solvent-cast 50 µm thick PVC film attached to a machined open-cell acrylic frame. Area 1 has a single 10 µl drop of protein solution and Area 2 has two 20 µl reservoir drops.

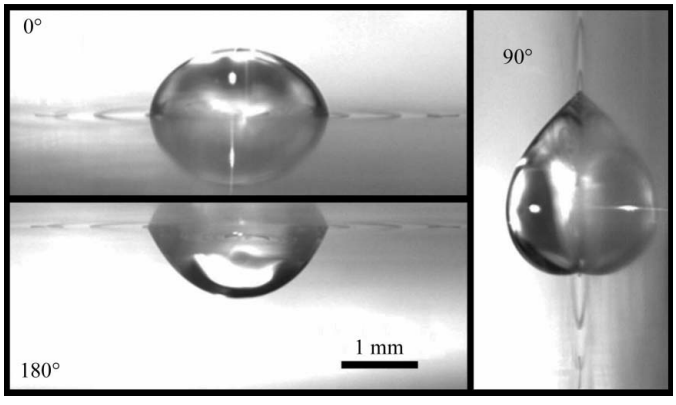

Figure 3
A 25 µl drop of DI water pinned to Area 1 of TDP plate prototype 1 immediately after dispensing (0°), after rotating the plate to the vertical (90°) and after inverting the plate to produce a hanging-drop (180°) configuration. The drop's contact line remains pinned to the same ring in all orientations.

bottom of a rigid 6.3 mm thick plastic/acrylic frame, as shown in Fig. 2. The frame defines and isolates individual cells for crystallization experiments. Unlike conventional crystallization plates, the plastic frame has an open-cell design and no wells for containing liquid drops. Instead, the protein and reservoir drops are held in place on the film by millimetre diameter, micrometre cross-section rings that strongly pin their contact lines. After filling, the plate is sealed by an unpatterned film applied to the top surface.

The bottom film pattern can be designed to match the needs of a particular class of experiments. Fig. 2(*a*) shows the first pattern used in our testing. The 6 mm diameter Area 1 consists of six 20 µm wide concentric rings with spacings of 250 µm between the inner two rings and 500 µm between the outer rings. These concentric rings allow pinning of protein drops with volumes ranging from ∼1 to ∼60 µl. The annular Area 2 surrounding these rings has four quadrants, each of which can hold up to ∼20 µl reservoir solution. Areas 1 and 2 are bounded by concentric groups of closely spaced rings (CSRs). These guard rings can catch the contact line if it depins from an inner ring (either owing to vibration or to a ring defect) and provide additional protection against drop spreading.

Fig. 2(*b*) shows an assembled plate with a central 10 µl protein drop and two 20 µl reservoir drops. The drops are dispensed in the sitting-drop configuration. As shown in Fig. 3, the strong contact line pinning provided by the rings allows the plate to be rotated 90° to the vertical (*e.g.* for X-ray data collection) or to be inverted for hanging-drop crystallization without any drop displacement. Locating the protein drop in the centre of each cell and surrounding it with reservoir solution maximizes the unobstructed solid angles for the incident and diffracted X-rays, maximizing the volume of reciprocal space accessible for data collection.

Because contact line pinning by micropatterned rings is so strong, drops with a wide variety of precisely controlled shapes can be produced. For example, a 'comet-shaped' drop produces evaporation-rate and concentration gradients that lead to nucleation rates that vary within the drop (Kalinin *et al.*, 2008). Crystallization by liquid–liquid diffusion can be implemented by connecting rings containing drops with different concentrations *via* a channel defined by two raised

Table 1
Comparison of maximum stable drop volumes V_{max} pinned to the 6 mm diameter ring of Area 1 on vertically oriented micropatterned PVC films of TDP plate prototype 1 and to an unpatterned vertically oriented PVC film for several aqueous solutions and liquids commonly used in protein crystallization.

Similar results were obtained on microembossed COC films; COC and PVC have very similar contact angles. For all liquids, the 14 µm high rings dramatically increase the maximum liquid volume that will remain pinned. CMC, critical micellar concentration. Jena Bioscience Detergent Screen solutions: D1-8, *N*,*N*-dimethyldodecylamine *N*-oxide (LDAO), CMC = 2 m*M*; D1-11, *N*-decanoyl-*N*-methylglucamine (MEGA-10), CMC = 7 m*M*; D2-5, *N*,*N*-dimethyldecylamine-*N*-oxide (DDAO), CMC = 10.4 m*M*; D2-10, *N*-octanoyl-*N*-methylglucamine (MEGA-8), CMC = 79 m*M*.

Liquid	V_{max}, 6 mm diameter ring (µl)	V_{max}, unpatterned PVC (µl)
DI water	60	15
PEG 4000, 30%(*w*/*v*)	40	10
2-Propanol, 20%(*v*/*v*)	30	5
tert-Butanol, 35%(*v*/*v*)	20	<1
Glycerol, 12%(*v*/*v*)	45	5
D1-8, CMC	20	1
D1-11, CMC	35	5
D2-5, CMC	20	<1
D2-10, CMC	15	<1

lines and then covering the drops with oil to minimize vapor diffusion.

The plate's frame, such as that of prototype 1 shown in Fig. 2(*b*), can be considerably simplified compared with more traditional plate designs. It need not have any optical quality surfaces and need not even be transparent. It can thus be made of any rigid material impermeable to water, alcohol and other volatile components of crystallization solutions. The same frame may be used with a variety of different film patterns.

3.1. Prototype 1 fabrication

The PVC films used in prototype 1 were made by solvent casting on a negative-image silicon wafer master (Siemann, 2005). The ring patterns on the master were designed using CAD software (*L-Edit*; Tanner Research Inc.) and negative masks were fabricated using a Heidelberg DWL 66 laser pattern generator capable of producing a minimum feature size of 500 nm. These patterns were then transferred to four-inch silicon wafers using photolithography. To remove any organic residues, the silicon wafer was first cleaned with a 6:1 Buffered Oxide Etch solution (Baker) and a boiling Nanostrip mixture (OM Group), washed with deionized (DI) water and then dried with N_2 gas. Next, the wafer was coated with a liquid primer [hexamethyldisilazane (HDMS; Shin-Etsu Chemical Co.) or P20 (Induron)] and then with Shipley SC1813 photoresist, both spun at 4000 rev min^{-1} for 30 s. The wafer was then baked on a hotplate at 388 K for 60 s, exposed through the mask to a UV dose of 33 mJ cm^{-2} using an EV620 contact aligner in soft contact mode, developed in AZ 300MIF (AZ Electronic Materials) developer for 45 s and then post-baked on a hotplate at 388 K for 60 s, leaving a patterned photoresist film with a thickness of ∼1.3 µm as measured with an optical interferometer. Patterns were etched through this masking film into the Si wafer to a depth of ∼15 µm (as measured by a Tencor P10 profilometer) using a Unaxis SLR 770 inductively coupled plasma/reactive ion etcher, which provides an etch rate of ∼1 µm per minute and an aspect ratio of 20:1. The photoresist was stripped from the etched wafers by soaking for 20 min in a 348 K bath of propylene glycol, *N*-methyl-2-pyrrolidone (NMP; BASF) and tetramethylammonium hydroxide (TMAH) and the wafers rinsed with DI water and dried with N_2 gas. Finally, to ensure full wetting and complete pattern transfer during solvent casting, the wafers were coated with a PEG monolayer using a molecular vapor-deposition tool (MVD100, Applied Microstructures), producing contact angles for DI water of ∼2° as measured with a VCA Optima XE tool. The side-wall angles of the final etched patterns, estimated using a Zeiss Ultra SEM, were 85°.

The patterned films were made of clear PVC (LXP-453; VCF Films Inc.). A 1:10 mixture of PVC dissolved in tetrahydrofuran (THF) was prepared by heating to 323 K and stirring at 400 rev min^{-1} for 15 min. This 'dope' was cast on a PEG-coated four-inch Si master and left to dry in a fume hood for 12 h. The resulting films were ∼50 µm thick and had patterned features 14.1 ± 0.3 µm high. The measured maximum advancing contact angle for DI water drops on flat films was 84 ± 1.3°. The side-wall angles as measured by a Tencor P10 profilometer (limited by the profilometer tip's angle) were >56°. The film was peeled off the wafer, cut to size and attached to the frame using high-vacuum grease.

3.2. Prototype 1 evaluation

The first prototype design was evaluated for its drop pinning, optical, UV and X-ray diffraction properties and was used for crystal growth and *in situ* X-ray analysis.

3.2.1. Film drop pinning properties. Micropatterned rings provide enhanced drop pinning and allow more precise control of drop shapes (Kalinin *et al.*, 2008). As shown in Fig. 3, relatively large-volume drops suitable for both protein and reservoir solutions can be dispensed on PVC films patterned with micrometre-tall rings and the film can then be rotated to the vertical and inverted to produce hanging drops without any motion of drop contact lines.

The pinning properties of cast PVC films with continuous circular rings were evaluated by dispensing drops onto the central Area 1 in Fig. 2(*a*). The liquids and solutions examined covered the range of properties encountered in protein crystallization, including DI water, 30%(*w*/*v*) PEG 4000, 12%(*v*/*v*) glycerol and ethylene glycol (used as cryoprotectants and viscosity enhancers in both globular protein and membrane-protein crystallization), 20%(*v*/*v*) 2-propanol and 30%(*v*/*v*) *tert*-butanol, several detergent solutions including 1% sodium dodecyl sulfate (SDS; used in membrane-protein crystallization) and Paratone-N oil (used to remove solvent and protect crystals from dehydration during X-ray examination). After dispensing, the films were rotated 90° from a horizontal to a vertical orientation and the maximum drop volume that remained stably pinned to Area 1 was determined.

Table 1 compares the maximum volumes for several liquids pinned to the largest (6 mm) diameter ring in Area 1 and to an unpatterned region of the PVC film. For all liquids, the patterned rings provide large enhancements in the maximum stable drop volume. The largest stable volumes were observed for DI water, but the largest fractional volume increases were for alcohol and detergent solutions, which have maximum advancing angles near 0° on unpatterned surfaces. Fig. 4 shows examples of drops having the maximum stable drop volume on vertically oriented patterned PVC films. In all cases the drop contact line is solidly pinned to the ring and retains its original contours during rotation without advancing or receding. These results imply that a single patterned film and thus a single crystallization plate can be used for both hanging-drop and sitting-drop crystallization with all common crystallization solutions.

The film rotations involved in generating Table 1 were quasi-static so as to determine the maximum stable drop volume. In crystallization practice, plate accelerations during routine manual and automated handling are much larger and so the maximum stable drop volumes (on both patterned and unpatterned surfaces) are smaller. The detailed drop dynamics in response to impulsive accelerations depend upon the drop volume and shape (which determine the ratio of inertial to pinning forces) and the liquid surface tension (which determines the energy stored in 'elastic' deformations of the drop), among other factors. An empirical rule of thumb is that for rings of a given diameter drop volumes of roughly 1/3 the maximum stable volume and smaller will be stable against routine impulsive accelerations. Because of the elastic 'snap' of the contact line when it depins from a ring, the closely spaced rings shown in Fig. 2(*a*) are more effective in preventing drop spreading for low-surface-tension liquids and solutions than for, for example, pure water.

3.2.2. Film optical properties. Aside from some optical distortion caused by variations in the cast film's thickness, 50 µm thick PVC films have good optical properties at both visible and UV wavelengths, with a transmittance greater than

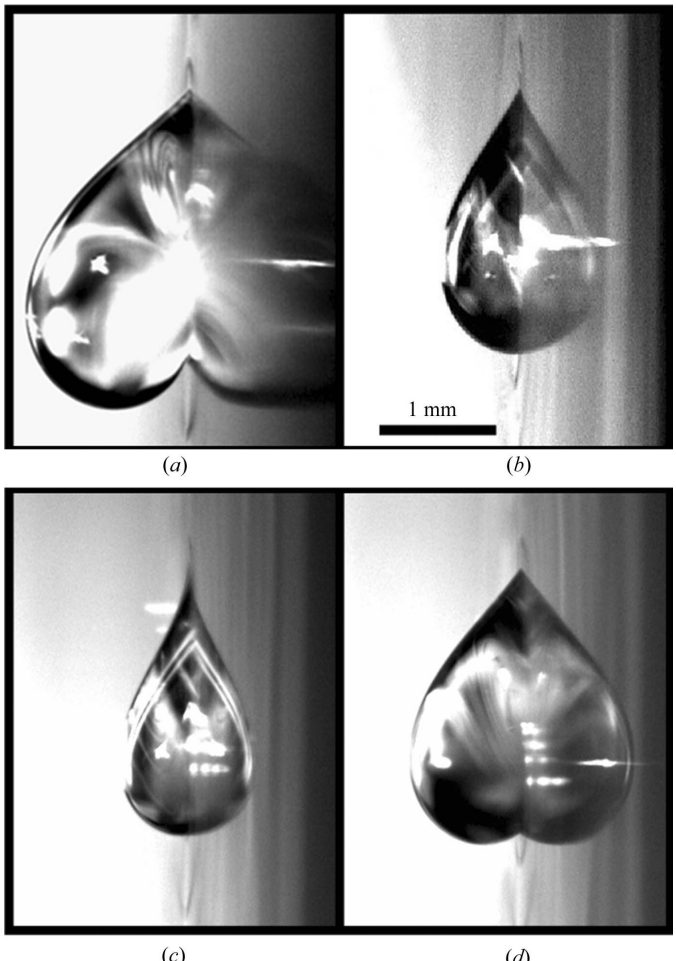

Figure 4
Images of the largest volume drop that remains pinned to rings on a micropatterned PVC film of prototype 1 when the film is rotated to a vertical orientation. (*a*) 60 µl DI water; (*b*) 15 µl Paratone-N oil; (*c*) 10 µl of a 1%(*w*/*v*) SDS solution; (*d*) 20 µl ethylene glycol.

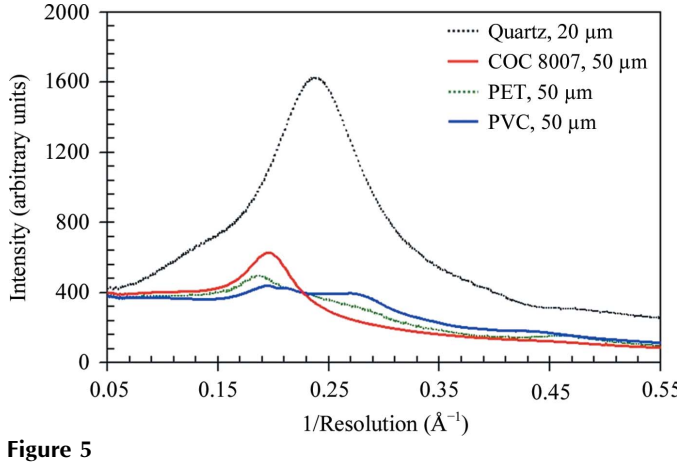

Figure 5
Diffuse X-ray scatter intensity *versus* resolution produced by directing a 12.7 keV X-ray beam through the 50 µm thick PVC film of TDP plate prototype 1, a 10 µm wall quartz X-ray capillary (20 µm total thickness), a 25 µm wall PET capillary (50 µm total thickness) and a 50 µm thick COC 8007 film from TDP plate prototype 2.

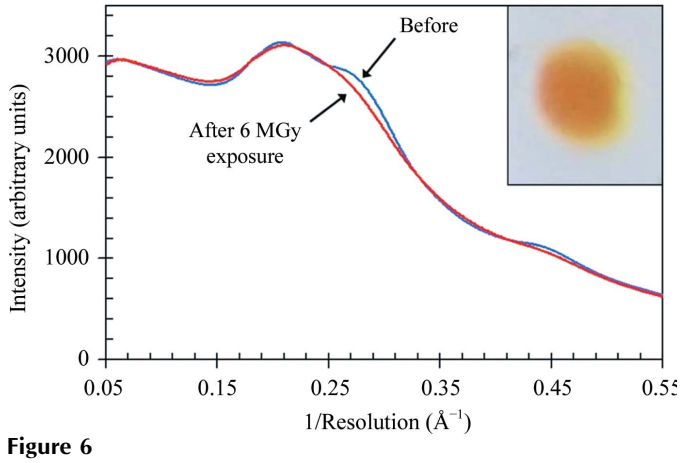

Figure 6
Diffuse X-ray diffraction intensity from a solvent-cast PVC film at room temperature after 1 and 10 min exposures to a 100 µm diameter 13.5 keV X-ray beam. The latter exposure delivered a dose of 6 MGy and resulted in the film discoloration shown in the inset, but produced little change in diffuse scatter.

85% for wavelengths of ≥250 nm. Because the polymer thickness in the plate is smaller (by a factor of 10–40) than in conventional injection-molded plates, a much broader range of polymers can give acceptable UV absorption.

3.2.3. Film X-ray diffraction properties. X-ray diffraction from the films was examined at the Cornell High Energy Synchrotron Source (CHESS) on beamlines A1 (λ = 0.98 Å, E = 12.7 keV) and F1 (λ = 0.92 Å, E = 13.5 keV) using a beam size of 100 µm. Fig. 5 compares the diffuse scatter from a 50 µm cast PVC film from plate prototype 1, a 10 µm wall quartz capillary (20 µm total thickness) and a 25 µm wall PET capillary (50 µm total thickness, from MiTeGen LLC) as a function of inverse resolution (Å^{-1}). The much thicker PVC film produces less diffuse background than the quartz capillary for the entire resolution range.

3.2.4. Film radiation damage. As with protein crystals, plastics are more susceptible to radiation damage at room temperature, where most crystal screening is likely to be performed, than at cryogenic temperatures. Fig. 6 shows how room-temperature irradiation affects the diffraction and optical properties of a solvent-cast patterned PVC film. The diffraction shows little change but, as shown in the inset in Fig. 6, the film's optical clarity in the irradiated region degrades after a dose (delivered to the film) of ∼6 MGy, corresponding to an incident fluence of 2.5×10^{12} photons in a 100 µm spot. This incident fluence would severely degrade diffraction from most protein crystals (Sliz *et al.*, 2003) and at the smaller fluences required for room-temperature diffraction screening visible damage to the film was slight.

3.2.5. Protein crystallization and drop visualization. Tetragonal hen egg-white lysozyme (HEWL) crystals were grown in plate prototype 1 by vapor diffusion at room temperature from a solution prepared by dissolving HEWL (20 mg ml^{-1}; Seikagaku America) and sodium chloride [7.0%(*w*/*v*)] in 0.1 *M* acetate buffer pH 4.5. A 10 µl drop of protein solution was dispensed into the

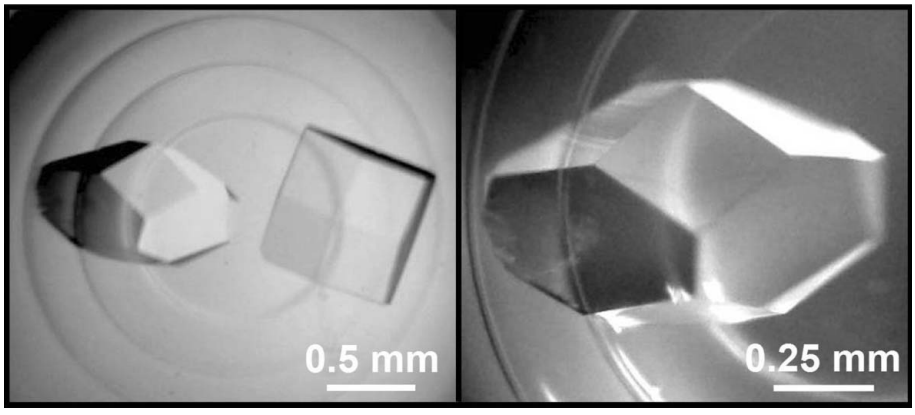

Figure 7
HEWL crystals grown in TDP plate prototype 1, photographed with the plate inverted and through the micropatterned solvent-cast PVC film.

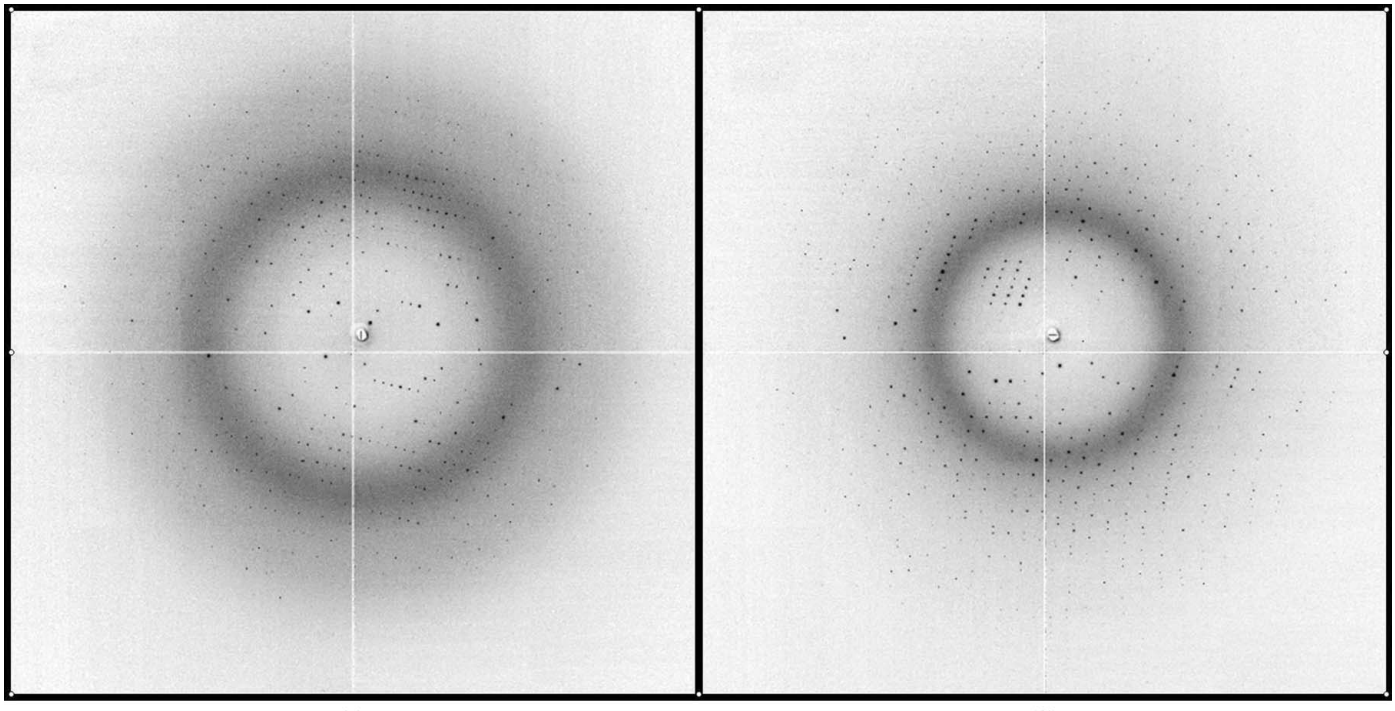

(*a*) (*b*)

Figure 8
Room-temperature X-ray diffraction patterns obtained from (*a*) a 200 µm lysozyme crystal grown and held in TDP plate prototype 1 surrounded by its original mother liquor and (*b*) the crystal from (*a*) harvested and mounted inside a 10 µm wall quartz capillary.

central Area 1 (Fig. 2), while two 20 µl drops of reservoir solution were dispensed in two quadrants of the surrounding annulus Area 2. The drops retained their perfect circular shape with no contact line recession during equilibration, during which the drop volume typically decreased by 50%. As shown in Fig. 7, the open obstruction-free cell design, the very thin, flat and optically clear film on which the drops rest and the small width of the rings results in excellent image quality, limited only by the effects of refraction arising from the drop's curved surface.

3.2.6. *In situ* protein crystal diffraction screening. To evaluate plate performance, crystal-containing plates were transported to CHESS and mounted vertically on the diffractometer at beamline A1. 5° scans (comprising five 1° oscillations) were recorded from crystals of different sizes. Each crystal examined was then harvested from the plate and placed inside a 10 µm wall quartz X-ray capillary and X-ray data collection was repeated. Fig. 8 compares the resulting diffraction patterns. The resolution and mosacity in the plate and in the capillary determined by *HKL*-2000 (Otwinowski & Minor, 1997) are essentially the same. The larger diffuse background visible for the plate arises from the mother liquor surrounding the crystal, little of which was transferred to the capillary.

3.2.7. *In situ* protein crystallography. The small plate thickness and the absence of well walls within each cell allow data collection over a wide range of incident and diffracted X-ray beam angles relative to the film normal. Complete diffraction data sets, involving 90 1° oscillations, were acquired at CHESS from lysozyme crystals grown in the plates and without any additional crystal manipulations. For a 600 µm lysozyme crystal suspended in its mother liquor, the maximum resolution determined by *HKL*-2000 at a crystal-to-detector distance of 125 mm was 1.42 Å and the data completeness was 99.9% in the resolution range 50–1.53 Å and 61.3% in the resolution range 1.47–1.42 Å.

3.2.8. Crystal retrieval for cryocrystallography. The highest quality and most complete data sets will generally be obtained from crystals cooled to $T \simeq 100$ K. *In situ* cryocooling using a cold gas stream or a cold thermally conducting rod to cool each drop is possible, but will produce relatively slow cooling and will require large cryoprotectant concentrations to prevent crystallization of the large volume of mother liquor surrounding the crystal. The highest quality diffraction data will generally be obtained by harvesting crystals from the plates, flash-cooling them and then collecting data using standard cryocrystallographic procedures. As expected, harvesting crystals from the plate prototypes was straightforward. Crystals could be grown in hanging drops, so that nearly all crystals were free-floating and very few adhered to the film. When crystals did adhere to the film, gentle pressure on the back of the film sometimes produced sufficient flex to release the crystals without damaging them. Current hanging-drop plates require that the drop-containing cover glass or film be cut out and removed from the plate and then inverted for harvesting, which can cause drop sliding and loss of crystals (especially in membrane-protein crystallization). With the present design, the plate is simply inverted after crystallization to produce a sitting drop and the crystals are harvested using standard methods.

4. Experiments and results: TDP crystallization plate prototype 2

TDP plate prototype 1 established the basic feasibility of crystallization plates based upon enhanced contact line pinning by topographic patterns. The next step was to fabricate and test designs closer to a practical implementation. Fig. 9 shows plate prototype 2, which consists of an injection-molded frame and a microembossed polymer film sealed to the frame bottom.

4.1. Prototype 2 design and fabrication

4.1.1. Frame design and prototyping. We chose to implement a 96-well SBS standard-format plate, which provides a good trade-off between experiment density and ease of crystal harvesting, is compatible with current plate-handling and sealing hardware and is currently the most popular commercial design. Initial prototypes were designed at MiTeGen with standard CAD software and were fabricated using stereolithography from Somos 11120 watershed clear resin. Once these designs had been validated, a final design modified for injection molding was produced at MiTeGen, molds were fabricated and 100 frames were molded. The final injection-molded frame is shown in Fig. 9(*a*).

The frame has an extremely simple open-cell design. Unlike conventional plates, none of its surfaces must be of optical quality. Nearly uniform polymer thickness and the absence of deep cavities facilitate uniform polymer cooling after injection and easy ejection from the mold, so a relatively simple mold can yield flat warp-free parts. These features should dramatically reduce the cost of final production molds. The total mass of polymer is roughly half that used in conventional plates, reducing both production cost and waste.

A variety of standard polymers can be used for the frame (including translucent and opaque polymers). We chose TOPAS 8007 COC (a cyclic olefin copolymer from TOPAS Advanced Polymers). Although relatively expensive, COC is used in many commercial plates because it has extremely low water absorption and water-vapor transmission and so maximizes the time filled plates can be stored without excessive drop dehydration. COC is also extremely stiff, which improves plate rigidity during automated handling. However, this choice is not crucial: most solvent loss typically occurs through the top sealing film, which is typically 10–20 times thinner than the frame and of a more permeable polymer.

Because there are no protein or reservoir solution wells, the central portion of the plate can be made very thin (3 mm in our prototype, limited only by the 'height' of hanging drops) and free of obstructions to incident and diffracted X-rays. Since both protein and reservoir solutions are confined within this thickness, convection and thus the rate of protein drop equilibration with the reservoir should be reduced [as occurs,

for example, during growth in glass capillaries (Adachi *et al.*, 2004)] and so should provide more gradual equilibration that is generally more favorable for nucleation of a small number of crystals. The protein drop and reservoir configurations are determined not by the frame, but by the micropatterned film that attaches to its bottom. Consequently, the same frame can be used for plates with one, two or three drops per cell (as shown in Figs. 9*b*–9*e*), different drop volumes and different reservoir configurations. This is a significant advantage over conventional plates, which require a new optical quality mold or mold insert for each design.

4.1.2. Microembossed films. The PVC films used in our first prototype have good but not perfect optical clarity and a moderate water-vapor transmission rate (WVTR) at 311 K of 4 g per 100 square inches per day per 25 µm thickness. For our commercial prototype, we used 100 µm thick TOPAS COC films, which have a much lower WVTR of ∼0.3 g per 100 square inches per day per 25 µm thickness at T = 311 K, allowing plates to be stored for much longer before the drops dry out. Direct measurements at room temperature on assembled plates with a 100 µm COC film sealing the plate bottom and 150 µm thick polyethylene microplate sealing tape (Corning 6524) sealing the top showed evaporation rates of ∼5 mg per day from the entire plate. At this rate, only 10% of a 10 µl reservoir volume will be lost in 20 d. The use of larger reservoir volumes should be unnecessary in most applications (Korczyńska *et al.*, 2007), reducing the cost of reagents.

To emboss the films, we developed a process using a Nanonex Nanoimprint Lithography (NIL) tool available at Cornell's Nanofabrication Facility, although conventional hot embossers can also be used. A Si-wafer master was fabricated as for the solvent-cast films and coated with 1*H*,1*H*,2*H*,2*H*-perfluorooctyltrichlorosilane (FOTS; Alpha Aesar) to reduce stiction. The COC film was stacked between this master and a

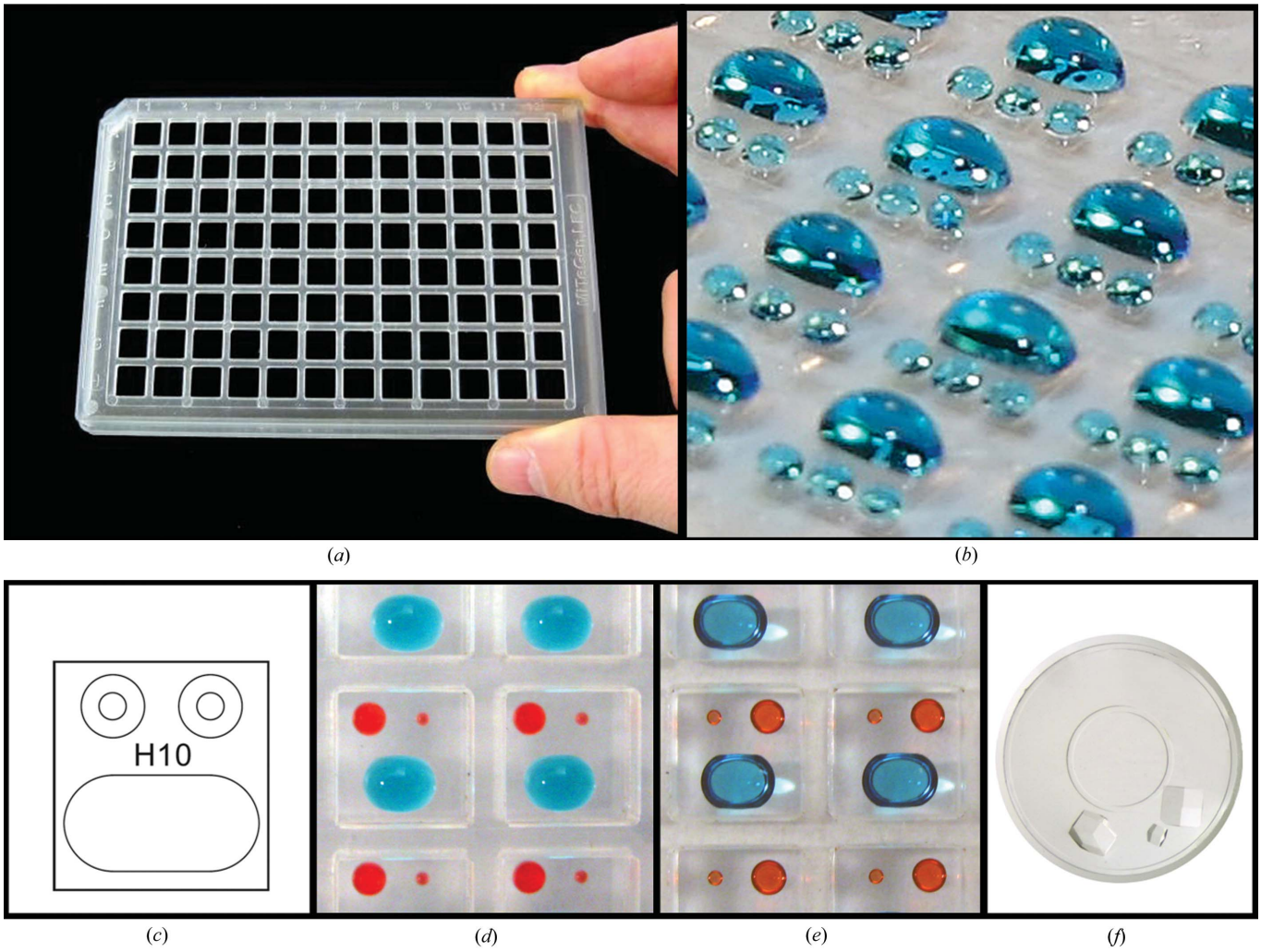

Figure 9
TDP plate prototype 2. (*a*) 96-well SBS standard open-cell frame injection-molded from COC. (*b*) 3 and 30 µl water drops manually dispensed on a three-drop microembossed 100 µm thick COC film. (*c*) Schematic diagram of the ring pattern in each cell of a two-drop prototype. The circular 'protein' rings are designed for drop volumes of 0.2 and 2 µl and the stadium-shaped 'reservoir' ring can hold up to 20 µl. (*d*) Water drops dispensed into plate prototype 2 using a Tecan automated liquid handler. The 'protein' drop volumes are 0.2 and 2 µl and the 'reservoir' drop volume is 15 µl. (*d*) The plate in (*c*) after inverting to obtain hanging drops. (*e*) Lysozyme crystals grown in the plate. Adhered crystals were removed by flexing the film.

flat Si wafer and inserted into the NIL tool. The film was first heated to 348 K with a pressure of 827 kPa and then embossed at 423 K with a pressure of 1.7 MPa. The resulting films had ring heights of ∼24 µm and ring side-wall angles of ≥56° as measured by a Tencor P10 profilometer.

4.2. Prototype 2 evaluation

4.2.1. Film drop pinning, optical and X-ray diffraction properties. Measured maximum advancing contact angles for DI water on flat COC films are 87 ± 1.8°, slightly larger than for PVC films. The embossed films have excellent drop pinning properties, with maximum advancing angles comparable to those in Table 1 for the solvent-cast PVC films. Fig. 9(*b*) shows an array of water drops manually dispensed onto a micropatterned COC film. The small circular drops have volumes of 3 µl and the elliptical reservoir drop has a 30 µl volume. Figs. 9(*d*) and 9(*e*) show an array of drops dispensed into an assembled plate using a TECAN automated liquid handler. The protein drops have perfect shapes and positions, as determined by the micropatterned rings. The reservoir drops in Figs. 9(*d*) and 9(*e*) remain stable in all orientations even with modestly rough handling. For reservoir drops having large concentrations of alcohols or detergents and thus small contact angles, the maximum stable drop volume and drop stability at a given volume are reduced. However, 10–15 µl volumes with good stability in routine handling, sufficient for crystallization experiments lasting at least one month, are still viable.

Unlike the solvent-cast PVC films, the microembossed COC films have essentially perfect optical clarity, providing excellent imaging of crystals, as shown in Fig. 9(*f*). The embossing process removes any scratches and other marks originally present on the film stock. COC films are also much stiffer than PVC films, which simplifies plate assembly.

As shown in Fig. 5, the diffuse X-ray background produced by the COC films is comparable in integrated intensity to that of PVC films, but has a somewhat smaller intensity at higher (*i.e.* numerically smaller) resolutions. The diffraction pattern is symmetric about the incident-beam direction, indicating that the polymer is unoriented. Except for the smallest protein drop volumes, the diffuse background is likely to be dominated by scattering from the mother liquor.

4.2.2. Automated drop dispensing and plate handling. In general, hand dispensing and plate handling is less precise and involves larger drop accelerations than automated dispensing, so one would expect the plates to perform especially well with automated drop dispensers. The drops shown in Figs. 9(*d*)–9(*f*) were dispensed using a TECAN multichannel dispenser. The plates have also been successfully tested with a Douglas Instruments Oryx liquid handler/protein crystallization robot and a TTP LabTech Mosquito dispenser and in both contact and noncontact dispensing modes.

The lightweight plate structure is rigid enough to perform well with automated plate-handling hardware. However, the plate lacks the arch-like support provided by the network of reservoir wells found on conventional plates. As a result, it shows more deflection when loaded in the middle and this can lead to poor plate sealing with automated sealers. This problem is easily overcome by simply modifying the plate holder to include an insert that supports the plate center. A less radical (and less versatile) plate design that includes conventional reservoir wells could also be adopted.

5. Conclusions

Topographic drop pinning provides new opportunities for the design of plates for protein crystallization and for other biotechnology applications involving dispensed liquid drops. Unlike surface patterns based upon, for example, differences in hydrophobicity/hydrophilicity, micropatterned rings having large side-wall angles but heights only a few percent of the drop heights can dramatically enhance contact line pinning for all solutions and liquids used in protein crystallization, including those used in membrane-protein crystallization. Rings result in dispensed drops with reliable shapes and positions, which is important for automated imaging and analysis of drop contents. They allow the drops to be rotated to any orientation and to survive the accelerations associated with routine handling without drop spreading or motion.

Use of micropatterned rings allows the plastic walls that confine protein drops in conventional plates to be eliminated. With these obstructions removed and the plate bottom replaced by a micropatterned thin film, a plate with unbeatable optical, UV and X-ray transmission properties can be obtained, allowing *in situ* screening of crystallization outcomes and lowest-background detection of microcrystals formed in early crystallization trials.

Micropatterned rings can also be used to stably hold substantial volumes of reservoir solution, allowing reservoir wells to be eliminated also. The plate's injection-molded frame can then be simplified to an open-cell design, reducing mold cost and plastic volume and reducing waste, while increasing the unobstructed solid angles for incident and diffracted X-ray beams. Sufficiently small reservoir volumes will remain stable in all orientations. The plate can then be inverted after filling for hanging-drop growth and/or mounted vertically for inspection using the horizontal X-ray beams produced by standard laboratory and synchrotron X-ray sources, eliminating the need for special plate scanners.

Smaller reservoir volumes will be more stable against the accelerations of routine handling, but will make water-vapor absorption and transmission by plate materials more critical. To maximize the duration of crystallization experiments, highly impermeable plastics should be used for the frame and top and bottom films. The plates can also be stored in a humidified environment: increasing the ambient humidity from 40 to 80% will increase experiment lifetime by at least a factor of three.

Crystallization plates based upon topographic drop pinning thus have the potential to resolve many of the problems associated with existing protein crystallization plates, while retaining full compatibility with existing liquid-dispensing and plate-handling hardware. Their new capabilities, especially for

ultra-low-background *in situ* X-ray inspection and hanging-drop growth of both soluble and membrane proteins, should help to increase the throughput of the protein-to-structure pipeline.

This work was supported by the NIH (R01 GM65981) and by a Phase 1 STTR award (R41 GM073278). The authors wish to acknowledge the assistance provided by Peter Schweitzer of the Genomics Core Facility at Cornell and by Patrick Stewart of Douglas Instruments Inc. Microfabrication work was performed at the Cornell NanoScale Facility, a member of the National Nanotechnology Infrastructure Network, which is supported by the National Science Foundation (grant ECS-0335765). X-ray diffraction measurements were performed at the Cornell High Energy Synchrotron Source (CHESS), which is supported by the National Science Foundation and the National Institutes of Health/National Institute of General Medical Sciences under NSF award DMR-0225180, and using the Macromolecular Diffraction at CHESS (MacCHESS) facility, which is supported by award RR-01646 from the National Institutes of Health through its National Center for Research Resources.

References

Adachi, H., Niino, A., Matsumura, H., Takano, K., Inoue, T., Mori, Y. & Sasaki, T. (2004). *Jpn. J. Appl. Phys.* **43**, 6264–6267.
Berejnov, V. & Thorne, R. E. (2005). *Acta Cryst.* D**61**, 1563–1567.
Bergfors, T. M. (1999). Editor. *Protein Crystallization: Techniques, Strategies and Tips*. La Jolla: International University Line.
Berry, I. M., Dym, O., Esnouf, R. M., Harlos, K., Meged, R., Perrakis, A., Sussman, J. L., Walter, T. S., Wilson, J. & Messerschmidt, A. (2006). *Acta Cryst.* D**62**, 1137–1149.
Bourgeois, D., Vernede, X., Adam, V., Fioravanti, E. & Ursby, T. (2002). *J. Appl. Cryst.* **35**, 319–326.
Chayen, N. E. (2007). Editor. *Protein Crystallization: Strategies for Structural Genomics*. La Jolla: International University Line.
Chayen, N. E. (2009). *Adv. Protein Chem. Struct. Biol.* **77**, 1–22.
Chayen, N. E. & Saridakis, E. (2008). *Nature Methods*, **5**, 147–153.
Cumbaa, C. A., Lauricella, A., Fehrman, N., Veatch, C., Collins, R., Luft, J. R., DeTitta, G. & Jurisica, I. (2003). *Acta Cryst.* D**59**, 1619–1627.
Dhouib, K., Khan Malek, C., Pfleging, W., Gauthier-Manuel, B., Duffait, R., Thuillier, G., Ferrigno, R., Jacquamet, L., Ohana, J., Ferrer, J.-L., Théobald-Dietrich, A., Giegé, R., Lorber, B. & Sauter, C. (2009). *Lab Chip*, **9**, 1412–1421.
Eisenstein, M. (2007). *Nature Methods*, **4**, 95–102.
Gavira, J. A., Toh, D., Lopéz-Jaramillo, J., García-Ruíz, J. M. & Ng, J. D. (2002). *Acta Cryst.* D**58**, 1147–1154.
Gerdts, C. J., Elliott, M., Lovell, S., Mixon, M. B., Napuli, A. J., Staker, B. L., Nollert, P. & Stewart, L. (2008). *Acta Cryst.* D**64**, 1116–1122.
Hansen, C. L., Classen, S., Berger, J. M. & Quake, S. R. (2006). *J. Am. Chem. Soc.* **128**, 3142–3143.
Hansen, C. L., Skordalakes, E., Berger, J. M. & Quake, S. R. (2002). *Proc. Natl Acad. Sci. USA*, **99**, 16531–16536.
Hiraki, M. *et al.* (2006). *Acta Cryst.* D**62**, 1058–1065.
Jacquamet, L., Ohana, J., Joly, J., Borel, F., Pirocchi, M., Charrault, P., Bertoni, A., Israel-Gouy, P., Carpentier, P., Kozielski, F., Blot, D. & Ferrer, J.-L. (2004). *Structure*, **12**, 1219–1225.
Jancarik, J. & Kim, S.-H. (1991). *J. Appl. Cryst.* **24**, 409–411.
Kalinin, Y., Berejnov, V. & Thorne, R. E. (2008). *Microfluid. Nanofluid.* **5**, 449–454.
Kalinin, Y. V., Berejnov, V. & Thorne, R. E. (2009). *Langmuir*, **25**, 5391–5397.
Kalinin, Y., Kmetko, J., Bartnik, A., Stewart, A., Gillilan, R., Lobkovsky, E. & Thorne, R. (2005). *J. Appl. Cryst.* **38**, 333–339.
Korczyńska, J., Hu, T.-C., Smith, D. K., Jenkins, J., Lewis, R., Edwards, T. & Brzozowski, A. M. (2007). *Acta Cryst.* D**63**, 1009–1015.
Leng, J. & Salmon, J. B. (2009). *Lab Chip*, **9**, 24–34.
Li, L. & Ismagilov, R. F. (2010). *Annu. Rev. Biophys.* **39**, 139–158.
Lu, Q.-Q., Yin, D.-C., Chen, R.-Q., Xie, S.-X., Liu, Y.-M., Zhang, X.-F., Zhu, L., Liu, Z.-T. & Shang, P. (2010). *J. Appl. Cryst.* **43**, 1021–1026.
McPherson, A. (1999). *Crystallization of Biological Macromolecules.* New York: Cold Spring Harbor Laboratory Press.
Otwinowski, Z. & Minor, W. (1997). *Methods Enzymol.* **276**, 307–326.
Sauter, C., Dhouib, K. & Lorber, B. (2007). *Cryst. Growth Des.* **7**, 2247–2250.
Shim, J., Cristobal, G., Link, D. R., Thorsen, T. & Fraden, S. (2007). *Cryst. Growth Des.* **7**, 2192–2194.
Siemann, U. (2005). *Prog. Colloid Polym. Sci.* **130**, 1–14.
Skarzynski, T. (2009). *Acta Cryst.* A**65**, s159.
Sliz, P., Harrison, S. C. & Rosenbaum, G. (2003). *Structure*, **11**, 13–19.
Stevens, R. C. (2000). *Curr. Opin. Struct. Biol.* **10**, 558–563.
Walter, T. S. *et al.* (2005). *Acta Cryst.* D**61**, 651–657.
Watanabe, N., Murai, H. & Tanaka, I. (2002). *Acta Cryst.* D**58**, 1527–1530.
Whon, T. W., Lee, Y.-H., An, D.-S., Song, H. K. & Kim, S.-G. (2009). *J. Appl. Cryst.* **42**, 975–976.
Yadav, M. K., Gerdts, C. J., Sanishvili, R., Smith, W. W., Roach, L. S., Ismagilov, R. F., Kuhn, P. & Stevens, R. C. (2005). *J. Appl. Cryst.* **38**, 900–905.
Zheng, B., Roach, L. S. & Ismagilov, R. F. (2003). *J. Am. Chem. Soc.* **125**, 11170–11171.